

Geological 3-D model of the larger Altensalzwedel area, Germany, for temperature prognosis and reservoir simulation

Ben Norden · Andrea Förster · Knut Behrends ·
Katja Krause · Lutz Stecken · Robert Meyer

Received: 15 December 2011 / Accepted: 28 April 2012 / Published online: 22 May 2012
© Springer-Verlag 2012

Abstract In the framework of the German R&D programme CLEAN (CO₂ Large-Scale Enhanced Gas Recovery in the Altmark Natural Gas Field), the geological structure of an area encompassing the Altensalzwedel sub-field and its surrounding was analysed in detail. A 3-D model was developed that contains the major geological formations and their general lithology including the natural gas reservoir (in the Permian Rotliegend), the immediate cap rock (Permian Zechstein) of the reservoir and its overburden. Based on this geological model, a 3-D steady-state thermal model was generated as part of a shared earth model. The parameterisation of the geological model layers with thermal rock properties is based on laboratory and well-log data. The model shows temperature changes in dependence of geological structure and of different rock thermal conductivity. The calculated surface heat flow is high (>80 mW m⁻²) for most of the area, which is in accordance to measured surface heat flow. Temperature on top of the Rotliegend reservoir is variable ranging from 110 to 150 °C. The quantification of temperature changes versus depth as well as laterally in the reservoir are valuable input data for modelling the dynamic processes of CO₂ injection within CLEAN.

Keywords CO₂ · 3-D modelling · Geological model · Temperature model · Altmark · Salt structures · Heat refraction

B. Norden (✉) · A. Förster · K. Behrends
GFZ German Research Centre for Geosciences,
Helmholtz Centre Potsdam, Telegrafenberg, Germany
e-mail: ben.norden@gfz-potsdam.de

K. Krause · L. Stecken · R. Meyer
GDF SUEZ E&P Deutschland GmbH, Lingen, Germany

Introduction

Fossil fuels still play a major role to meet mankind's energy demands. However, due to increasingly limited resources and environmental aspects, research on the exploration and the use of regenerative energy sources is progressing. A technology thought to build a bridge between the utilisation of greenhouse-gas emitting fossil fuels and of regenerative “green” energy (see e.g. Haszeldine 2009) is the so-called CCS technology, which stands for “Carbon Dioxide Capture and Sequestration/Storage”. The idea behind CCS is to capture one of the most relevant greenhouse gases (carbon dioxide, CO₂) and store it in the underground instead of emitting the gas into the atmosphere. Due to the proven record of gas containment in gas fields sealed by impermeable cap rocks, nearly exploited gas reservoirs may be seen as an obvious target for the CO₂ underground storage at large scale. The almost depleted Altmark gas field in Germany, which once was the second largest on-shore gas field in Europe, is such a desired target (Kühn et al. 2012).

The Altmark area is situated in the Northeast German Basin (NEGB), which represents a sub-basin of the southern Permian Basin in Europe, extending from England to Poland (Ziegler 1990). The Altmark gas field covers an area of more than 1,000 km² (Fig. 1). The natural gas is contained in Permian Rotliegend clastic rocks sealed by Zechstein rocks, comprising thick layers of rock salt (Fig. 2). The reservoir, having had initially about 9.4 Tcf of gas in place, has reached a recovery degree of more than 78 % (Rückheim et al. 2005).

Given the mature state of the reservoir, it is desirable to extract the remaining gas by using a CO₂-based enhanced gas recovery (EGR) technique. The application of such a technique would have benefits that are twofold. First, it



Fig. 1 Map of central Europe, covering the northern part of Germany and the western part of the Netherlands and showing major gas fields (in red) and Zechstein salt structures (in dark blue) (after LBEG 2010). Also shown is the area of the Altmark gas field with its different compartments (sub-fields): A Salzwedel, B Riebau,

C Peckensen, D Altensalzwedel, E Heidberg, F Zethlingen, G Mellin, and H Winkelstedt (after Müller 1994). The rectangle marks the area for which both a geological and a thermal model were generated. S59 marks the location of a borehole for which a presumably unperturbed temperature log is available

would have an economic bearing for the gas field operator and second, in-depth studies accompanying the production process would be beneficial to prepare for any future CO₂ storage planning. These are also the goals around those the agenda of the CLEAN project (Kühn et al. 2011, 2012) was centred, for which the Altensalzwedel sub-field (Fig. 1) was selected as a target area for a pilot CO₂ injection.

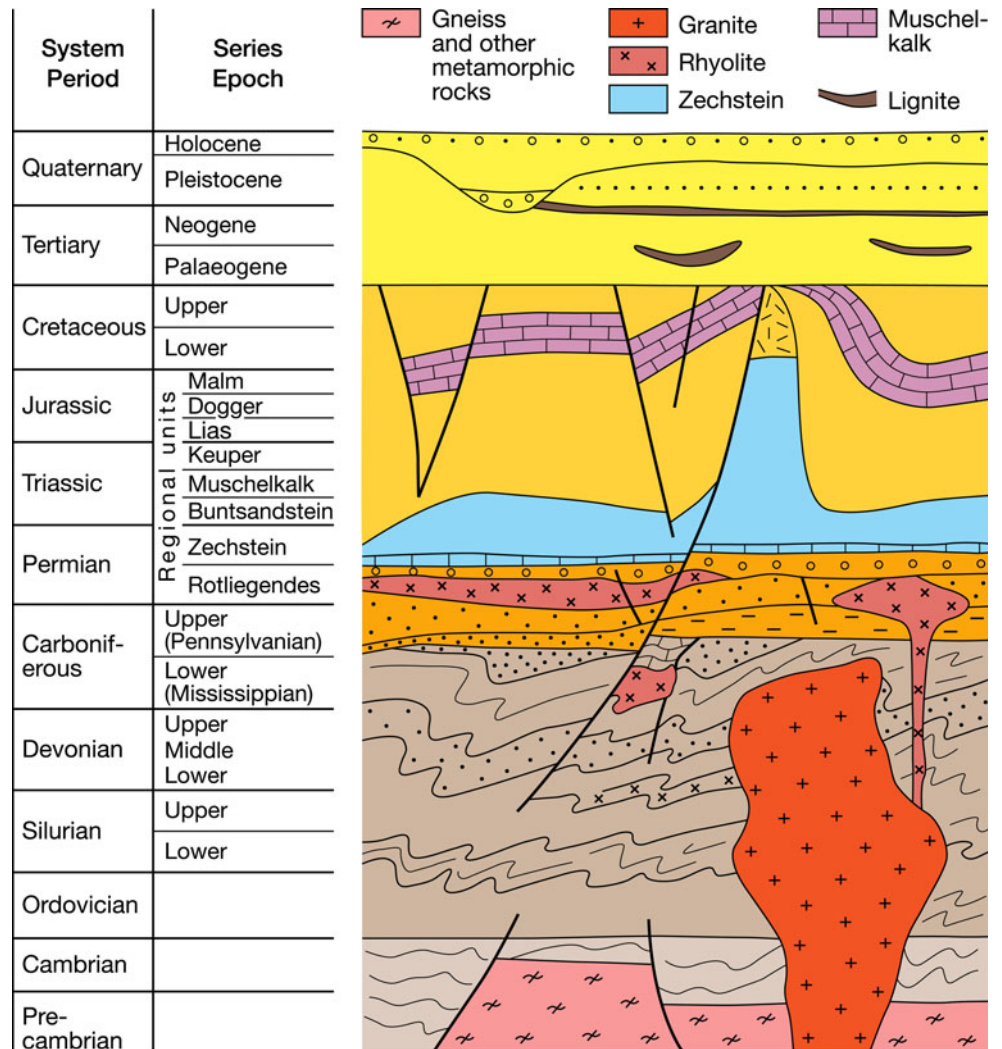
In this paper, we present a geological and geothermal baseline characterisation from local to regional scale for the larger Altensalzwedel area of an overall size of 350 km². The structural model is based on the huge amount of legacy data available from hydrocarbon exploration and production, e.g. interpreted seismic profiles, borehole reports, structural maps, and other regional maps as well as literature data. The geological model covers the gas reservoir, its cap rock and the remaining overburden, and includes the basement to a depth of 10 km. It reflects the structural features, such as existing faults, as well as a generalised lithology. For the thermal modelling, a proper parameterization of the structural model was necessary. For this purpose, laboratory measurements of thermal conductivity were conducted on available cores from the Altensalzwedel boreholes to supplement thermo-physical data available from literature. In addition, cross-correlations using available high-resolution, thermally undisturbed temperature logs from other locations in the NEGB were used for the assessment of thermal rock properties.

The 3-D temperature model is generated by using the 3-D finite differences software Processing SHEMAT (Simulator for Heat and Mass Transport, Clauser 2003). The thermal modelling is conducted as a reconnaissance approach for the prediction of the thermal field on a regional scale. Although SHEMAT is capable of solving the coupled equations for fluid flow, heat transfer, and mass transport in saturated porous media (e.g. Kühn et al. 2002; Vedova et al. 2008), we applied for the reconnaissance a conductive steady-state model, honouring the limited available data (see e.g. Mottaghy and Pechinig 2009). Fluid flow through geological formations (aquifers) as well as along faults is not considered. In SHEMAT, the implemented heat transfer equation reads then:

$$0 = \nabla(\lambda_g \nabla T) + H \quad (1)$$

where T (°C) denotes temperature and λ_g (W m⁻¹ K⁻¹) the bulk thermal conductivity. H (W m⁻³) summarises the heat sources such as constant basal heat flow at the lower boundary, rock heat production rate, and global fluid heat production rate. Matrix rock and fluid thermal conductivity are weighted after the geometric mean with the porosity Φ to bulk thermal conductivity. In addition, the code takes the temperature dependence of rock thermal conductivity into account by using the formula of Zoth and Haenel (1988). Although thermal rock capacity is not needed for the steady-state simulation, estimations of this parameter are

Fig. 2 Simplified geological section of the Altmark region including stratigraphy (after Radzinski 1996 and DSK 2002)



also reported later on for the sake of completeness of the thermal characterisation.

In the following, the available database for the structural model is presented. Thereafter, a brief description of the lithology and the associated thermal properties of the lithological units are given and the set-up of the thermal model and the applied boundary conditions are presented. Although the results of the combined geological and thermal model are used in the preparation of EGR operations, they would also be supportive for any other future activity of using the underground, for example for the exploration and exploitation of geothermal resources in saline aquifers above the exploited gas reservoir.

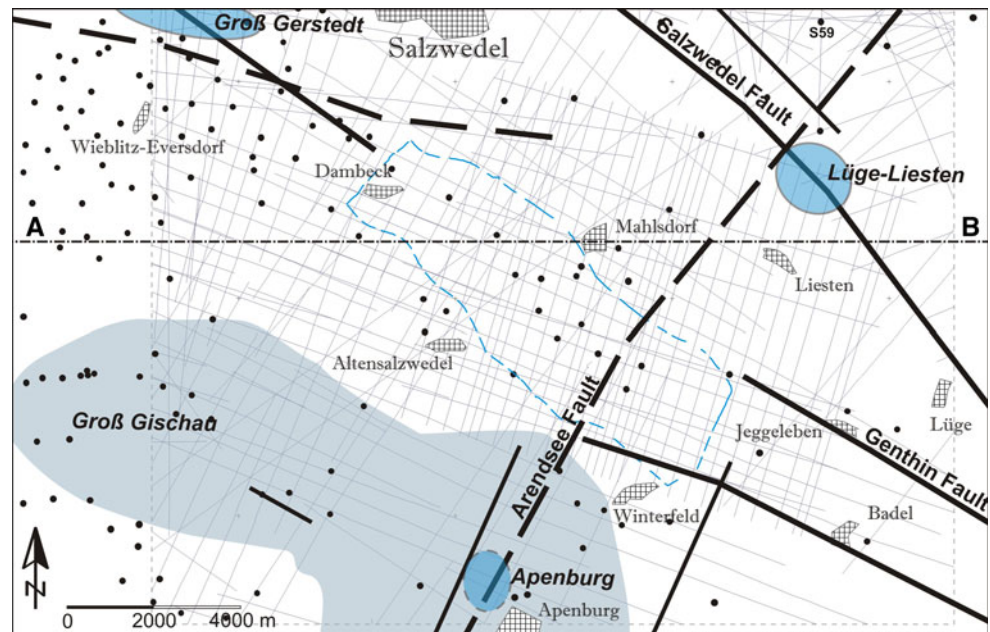
Basis data

The study benefited from the huge amount of available in-house data of GDF SUEZ E&P Deutschland GmbH. The data set includes interpreted seismic sections and records of

approximately 150 deep boreholes, partially including petrophysical well logs (Fig. 3). The data cover the subsurface down to the Rotliegend reservoir at about 3.7 km depth. Public domain data (e.g. regional structural maps) supplement the database for the deeper subsurface below the Rotliegend; however, data from this depth are rare.

Thermal conductivity was measured on 40 core samples, covering Permian anhydritic rock, mudstones, siltstones and sandstones from three boreholes located within the study area. In addition, thermophysical data available from literature were used (Balling et al. 1981; Čermák et al. 1982; Effenberger 2000; El-Sharkawy et al. 1984; Fuchs and Förster 2010; Hamdan and Clarke 2010; Hjuler and Fabricius 2009; Hölting 1996; Lotz 2004; Norden and Förster 2006; Norden et al. 2008; Otto 2010; Pechnig et al. 2009; Schön 1996; TU München 2010; UEIS 2010; VDI 2000). Finally, thermal conductivity also was determined from cross-correlation with other locations within the NEGB, for which a high-resolution, thermally undisturbed temperature log is available.

Fig. 3 Geographic map of the model area with locations of salt structures (in gray) and of main Mesozoic faults (thick lines) based on seismic data and LAGB (2011). Line A, B refers to the cross-section shown in Fig. 4; the stippled line indicates margins of the Altensalzwedel sub-field. Shown are location of deep boreholes and the location of 2-D seismic lines available for this study, highlighting the excellent data coverage for the study area



In contrast to the huge amount of structural data, reliable temperature data in this region are scarce. Only for one well, the S59 borehole, an undisturbed temperature log is available with temperature readings of 50-m intervals in the depth range from 200 to 3,650 m b.g.l. Additional thermal data are provided by bottom-hole temperatures (BHTs). However, the BHTs are regarded as poor information as the data are influenced by the drilling process and the circulation of the drilling mud. Even if corrected in some way for these processes, BHTs are regarded as less reliable since the parameters needed for the correction usually are not fully available (e.g. Speece et al. 1985; Jessop 1990; Deming 1989; Förster 2001). For this study, empirically corrected BHTs were available from seven borehole locations west of the S59 borehole (Lorenz 1971) (Fig. 3). Other single temperature data, such as temperature measurements from drill stem tests (DSTs) were not available.

Model set up

Geological structure

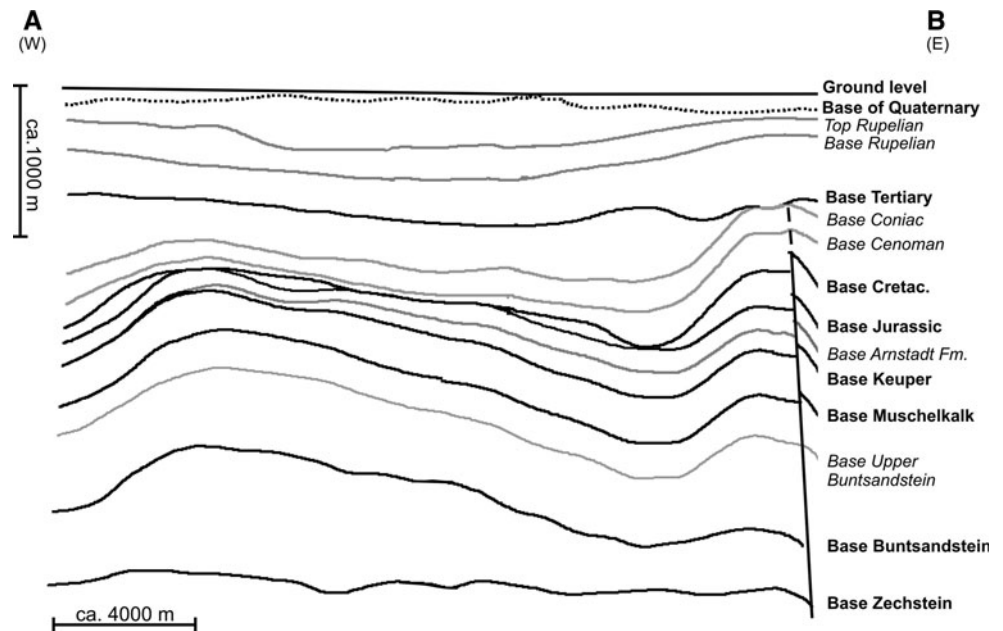
The deepest part of the model from 10 km to about 5.5 km represents the basement of the Permian basin (Scheibe et al. 2005). The structural layering of the basement units is practically unknown. Rocks of Ordovician to Carboniferous age comprise the upper part of the basement to depths of about 5–6 km (4.5 km in the western part of the Altmark; Stottmeister and Poblozki 1999). The basement is intersected by faults, which originated during the late

Carboniferous to early Rotliegend times by regional warping. The faults are oriented from NNE–SSW to NE–SW (Rhenish to Variscan) and NW–SE (Hercynian). Tectonic instability increased during the late Stephanian resulting in a large, basin-wide volcanic activity (Benek et al. 1996). Volcanic rocks, and subordinately terrigenous sediments, form the Upper Carboniferous to Lower Rotliegend (Lower Permian) Altmark subgroup. The depth of the base of the volcanic rocks on top of the crystalline basement was determined by adding the thickness of the Permocarboniferous volcanic rocks to the modelled base of the sedimentary Rotliegend (next paragraph). According to Benek et al. (1996), the volcanic rocks show a mean thickness of 1,300 m.

The Upper Rotliegend post-volcanic sedimentation started after a hiatus. Tectonic movements are responsible for the variable thickness of the Rotliegend sediments in the Altmark area (80–830 m; Stottmeister and Poblozki 1999). The average depth of the base of the Upper Rotliegend determined from available borehole data and geological maps (e.g. Bachmann et al. 2008) amounts to about 3,700 m in the whole model domain and is in the order of 3,600 m in the Altensalzwedel sub-field (stippled line in Fig. 3).

The base of the cyclic evaporitic Zechstein in the study area is located at depths between 3,200 and 3,500 m. The primary thickness of the Zechstein Formation (i.e. mainly the Stassfurt halite and the Leine cycle) amounts to about 900–1,100 m (Benox et al. 1997). The Zechstein constitutes the immediate cap rock of the Rotliegend gas reservoir. Above the Zechstein salt, Mesozoic to Cenozoic sediments form the supra-Zechstein salt succession.

Fig. 4 Generalized geological structure of the overburden of the Rotliegend gas reservoir sliced from the 3-D geological model. Trace of section shown in Fig. 3



The Zechstein salt started to move along zones of structural weaknesses as the weight of the overburden increased (Trusheim 1957; Fig. 2) thus complicating the geological structure in the area. The Zechstein salt moved upwards, where the Mesozoic Arendsee, Salzwedel, and Apenburg-Wernstedt fault zones intersect each other (Fig. 3). Three salt structures can be distinguished: the Lüge-Liesten and the Apenburg salt diapir and the Groß Gischau salt pillow (Fig. 3). Their evolution controlled the deposition of the sediments since the Triassic. Whereas the base of Zechstein represents a continuous and more or less flat surface, the top of the Zechstein formation is, due to different degrees of salt mobilisation, irregular. The Zechstein salt thickness is <200 m in zones, from which salt migrated away, to >2,500 m in the Lüge-Liesten salt diapir, where the salt is accumulated to a depth of about 250 m below surface. For the Apenburg salt diapir, which is not fully resolved by the seismic data it is assumed that its top is situated at a depth of 300–400 m below surface.

The Triassic Buntsandstein and Muschelkalk units show a more or less uniform thickness: the Lower and Middle Buntsandstein unit is about 500 m thick, the Upper Buntsandstein about 250 m, and the Muschelkalk about 300 m, respectively. The entire sedimentary sequence is deformed due to the salt migration into gentle anticline and syncline structures. Where salt diapirs penetrated the Triassic, the geological structure is deformed more intensively. The units overlying the Muschelkalk show thicknesses that are different across the area but follow a consistent trend (Fig. 4). The Erfurt and Grabfeld Formations (Upper Triassic Keuper), partly absent in the northwestern part of the model, show an increasing thickness from <10 m (at

Wieblitz-Eversdorf) to >220 m in the eastern part of the model around the Salzwedel fault system. Similarly, the Arnstadt and Exter Formations show thicknesses of <50 m in the west and >400 m in the east. The Stuttgart Formation is not present in the study area.

Lower Jurassic sediments (Lias) are less prominent in the study area. They are missing in areas of local highs (e.g. at the Groß Gischau salt pillow, Figs. 3, 4, showing the margin of the salt pillow) and can elsewhere reach thicknesses of up to 180 m. In the west of the Salzwedel fault system, Jurassic sediments show a maximum thickness of about 300 m. Similarly linked to salt features is the thickness of the Cretaceous sediments. In elevated areas, sediments were never deposited or later eroded completely, whereas in depression zones the sediment thickness can reach values of >1,250 m.

The Tertiary ingresson surface is less affected by salt structures and fault systems. The Tertiary is between about 400 and 800 m thick. The Oligocene Rupelian, with the Rupelton acting as a regional aquitard, has thicknesses of 150 m to >200 m (Fig. 4).

Quaternary sediments show a mean thickness of 25 m, but achieve higher values in areas where glacial incision troughs cut into the underlying units. Close to Jeggeleben (between the villages of Winterfeld and Lüge) such an incision trough cuts also into the Rupelton, reducing its thickness to values of less than 60 m.

Lithology and petrophysical properties

In order to assess representative thermal properties for the units of the geological model, the lithologies and their

related characteristic thermo-physical properties were investigated in more detail. The lower part of the basement consists most likely of metamorphic rocks (gneisses) and felsic intrusive rocks (Fig. 2), whereas the upper part of the basement to depths of about 5.5 km is assumed to consist of greywacke, argillaceous schist, diabase, and limestone (Stottmeister et al. 2008). Due to a lack of core, the thermo-physical properties of these units are difficult to estimate. We used the results from Lotz (2004), Norden and Förster (2006), and Norden et al. (2008) and assigned an average matrix thermal conductivity of $3.1 \text{ W m}^{-1} \text{ K}^{-1}$ and a heat production rate of $2.3 \mu\text{W m}^{-3}$ to the basement complex.

The volcanic rocks above the basement consist of andesites, ignimbrites, rhyolites, and basalts, reaching a thickness of >2 km (Benek et al. 1996; Bachmann et al.

2008). The volumetric composition of the Altmark volcanic rocks provided by Benek et al. (1996) and the thermo-physical properties given by Norden and Förster (2006) gave rise to average values of thermal conductivity and radiogenic heat production of $2.8 \text{ W m}^{-1} \text{ K}^{-1}$ and $2.9 \mu\text{W m}^{-3}$, respectively.

The much better borehole control for the overburden of the Permocarbiniferous rocks allows a more detailed thermal characterisation of the lithological units. Based on the borehole records made available in a digital form within the CLEAN project, the lithological and stratigraphic description of 67 wells was analysed. For the post-Permocarbiniferous sedimentary succession, twelve thermo-physical stratigraphic units (Table 1) and twelve different mean rock types were distinguished (Table 2).

Table 1 Thermal units of the 3-D model and listing of the corresponding model layers (see Table 6) and the maximum depth range of the assigned thermal unit properties

Unit	Corresponding stratigraphy	Layer no.	Max. depth range (m)
1	Quaternary to Tertiary (Chattian)	1–8	0–500
2	Tertiary (Rupelian)	2–9	50–600
3	Tertiary (Eocene to Palaeocene)	5–12	200–900
4	Cretaceous	7–22	300–1,900
5	Jurassic (Lias)	8–24	400–2,100
6	Keuper (Arnstadt & Exter Fm.)	10–26	600–2,300
7	Keuper (Grabfeld & Erfurt Fm.)	12–27	800–2,400
8	Muschelkalk	12–30	800–2,700
9	Upper Buntsandstein	14–33	1,000–3,000
10	Lower and Middle Buntsandstein	17–36	1,300–3,300
11	Zechstein	5–37	200–3,450
12	Rotliegend	35–40	3,100–3,900
13	Permocarbiniferous	38–48	3,450–5,500
14	Proterozoic to Westfalian (prae-Stefanian)	43–57	4,200–10,000

Table 2 Mean composition (in per cent) of the units 1–12 based on borehole data

Mean rock type	1	2	3	4	5	6	7	8	9	10	11	12	Total
Anhydrite								2	10		17		2
Limestone				22				48			1		6
Lignite	10												1
Marl	6	2											1
Marlstone				69	10	17	19	37	19				14
Rock salt								8	35		79		10
Sand	57	4	23										7
Sandstone				2	35	16	6		2	6		46	9
Silt	19	14	44										6
Siltstone				2	15	24	28		16	34		44	14
Clay	7	80	32										10
Mudstone				5	40	41	46	3	18	60	3	10	19
Total	99	100	99	100	100	99	99	99	99	99	99	100	100

For unit codes see Table 1

The thermal conductivity, heat capacity and porosity of the mean rock types were determined either by laboratory measurements and/or by analysis of well-log data, and from analogue studies and literature data.

For the Rotliegend reservoir section, new laboratory measurements on core samples were used. Thermal conductivity (TC) was measured on 39 dry or pseudo-dry samples using the TC/thermal diffusivity scanning device (Popov et al. 1999; Table 3); on a subset of samples also thermal diffusivity (TD) was measured. An empirical correction was applied to relate the values to those for oven-dried conditions. Porosity (Table 3) was either measured using helium gas (Pudlo et al. 2012) or water, following the Archimedes principle, or was estimated. In thermal modelling, bulk thermal properties are often calculated based on matrix thermal conductivity, porosity, and the respective pore content. Therefore, matrix TC (Table 3) and matrix heat capacity were calculated based on porosity and air- or water-saturated measured (bulk) values using the geometric mean model. Calculated matrix values for the heat capacity of all rocks are in the range of 1.1–2.6 MJ m⁻³ K⁻¹ (not shown in Table 3). The new data was integrated into the available data from the sedimentary Rotliegend (Norden and Förster 2006) to derive representative rock thermal properties for Permian mud-, silt-, and sandstones (Table 4).

To circumnavigate the lack of cores to characterise the thermo-physical properties of the post-Permian succession of the Altmark area, mean rock thermal properties for every stratigraphic unit (Table 2) were estimated using additional data (Table 4). In addition to literature data, TC, for example, was estimated by using undisturbed continuous temperature profiles (T) in conjunction with known heat flow (q) at other sites of the NEGB. If additional heat sources could be neglected, TC could be calculated using $q = TC \times dT/dx$ (see e.g. Fuchs and Förster 2010). Heat capacity was estimated using literature data; rock density was calculated based on well-log data and published reports and compilations. For several borehole locations of the Altmark, the well-log responses of the sonic and gamma-ray measurements were compared with the well-log derived TC data of boreholes with known temperature distribution. Thus, a more reliable estimation of the present rock thermal properties was facilitated forming the basis for the mean thermal properties for the respective thermal units of the model (Table 5, next section). The heat production of the units was parameterised using the data given by Lotz (2004) and Norden et al. (2008).

Thermal model construction

The 3-D model was generated for the greater Altensalzwedel area situated between Salzwedel in the north and the village of Apenburg in the south (Fig. 3).

In total, 57 model layers and 14 thermo-physical units were used to incorporate the geological model into SHEMAT. The grid size of the model is 100 m × 100 m in horizontal direction. In vertical direction, the grid size varies between 150 and 500 m in the lower model section and between 50 and 100 m in the upper model section (Table 6). The 14 thermo-physical units of the conceptual model represent main stratigraphic units of a typical rock composition (Tables 1, 2, 5). The lowermost two units comprise the basement and the Permocarboniferous volcanic rock complexes, respectively, whereas the other units represent the sedimentary section of the basin. To establish convenient thermal boundary conditions for the thermal modelling, the model was constructed to a depth of 10 km.

In the finite-differences software SHEMAT, all model layers are continuously present in the whole model domain. Thus, geological structures interrupting the horizontal strata represented by the model layers were incorporated by assigning the respective model cells above the layer with the appropriate thermal properties. For example, salt structures are incorporated by assigning the thermal properties of salt instead of the “normal” rock thermal properties of the overburden for the model cells “affected” by the updoming of salt. Thus, model cells representing the salt structure above the “salt layer” obtain the thermal properties of salt. Practically, the respective thermo-physical properties for every cell of one model layer were assigned based on the distribution of the units in the corresponding depth slices of the geological model.

Thermal boundaries

For the upper model boundary, a constant temperature of 10 °C was used. The lower model boundary at 10 km depth is defined by a heat-flow value of 70 mW m⁻², which is based on a heat-flow study by Norden et al. (2008). At the side boundaries of the model, the horizontal temperature gradients are assumed to be zero (no horizontal heat transfer).

Results

Thermal conductivity

Thermal conductivity determined for different rock types differs with respect to stratigraphic unit (Table 4). Whereas the porosity of lithotypes generally decreases with stratigraphic age (burial depth), the values of the matrix TC values are more variable. For example, the matrix TC of sandstones differs from 2.4 to 5.4 W m⁻¹ K⁻¹, resulting in bulk TC values in the order of 2.1–3.4 W m⁻¹ K⁻¹, depending on the respective porosity. The variability of the

Table 3 New thermal conductivity (TC, $\text{W m}^{-1} \text{K}^{-1}$) data of Altmark samples (ss, sandstone; si, siltstone; ms, mudstone; ah, anhydrite; na, halite) determined by laboratory measurements for the Rotliegend and the Zechstein (sample no. 26)

Sample-ID	Lithology	Porosity (%)	Oven-dried measurement			Saturated measurement			Direct measurement			Matrix TC (cb/ct)	Matrix TC (f)
			cm TC	cb/ct TC	<i>f</i> TC	cm TC	cb/ct TC	<i>f</i> TC	cm TC	cb/ct TC	<i>f</i> TC		
26	an/ha	0.4	5.3	5.5	5.6	5.6	5.2	5.1	5.1	5.4	5.3	5.2	5.7
5	ms	1.5	1.9	2.2	2.2	1.8	2.0		2.3	2.2		2.1	2.4
20	ms	1.4	2.1	2.5	2.4	1.1	1.9		2.3	2.4		1.9	2.6
22	ms	0.3	2.8	3.3	3.0	2.5	2.9		3.1	3.1		2.9	3.0
15	ms and si	1.8	2.3	2.3	2.6	2.2	1.6		2.7	2.3		1.7	2.9
10	ms, silty	0.6	1.9	2.3	2.3	1.8	2.0		2.5	2.3		2.1	2.4
27	ms, silty	3.2		2.5	3.1	3.0	3.0	3.3		2.5	3.2	3.1	3.7
3	ss	<i>19.4</i>	<i>2.1</i>	<i>1.8</i>	<i>2.4</i>				2.2	1.9			7.1
4	ss	<i>20.3</i>	<i>1.8</i>		<i>2.2</i>				2.0				6.7
8	ss	<i>2.7</i>	<i>3.1</i>		<i>3.3</i>				3.1				3.8
9	ss	<i>19.3</i>	<i>1.5</i>		<i>1.9</i>				1.7				5.4
12	ss	<i>20.2</i>	<i>1.4</i>		<i>1.8</i>				1.6				5.3
13	ss	<u><i>15.0</i></u>	<i>1.9</i>		<i>2.3</i>				2.1				5.0
16	ss	<u><i>6.3</i></u>	<i>2.9</i>		<i>3.1</i>				2.9				4.3
17	ss	<i>4.1</i>	<i>3.1</i>		<i>3.3</i>				3.1				4.1
18	ss	<i>15.5</i>	<i>2.2</i>		<i>2.5</i>				2.3				5.8
21	ss	<i>11.9</i>	<i>2.7</i>		<i>2.9</i>				2.7				5.6
23	ss	<i>8.9</i>	<i>2.9</i>		<i>3.1</i>				2.9				5.0
25	ss	<i>5.3</i>	<i>3.1</i>		<i>3.3</i>				3.1				4.4
33	ss	<u><i>10.0</i></u>	<i>2.9</i>		<i>3.1</i>				2.9		3.1		5.4
34	ss	<u><i>10.0</i></u>	<i>2.1</i>		<i>2.2</i>				2.2		2.3		3.6
36	ss	<u><i>10.0</i></u>	<i>2.6</i>		<i>2.6</i>				2.6		2.6		4.3
38	ss (patchy)	<u><i>10.0</i></u>	<i>1.9</i>		<i>1.9</i>				2.1		2.0		3.0
14	ss to ms	<i>0.9</i>	<i>3.2</i>		<i>3.4</i>				3.2				3.6
19	ss, homogenous	9.9	2.5	3.5	3.2		4.7	4.1	2.8	3.3	3.1	5.9	5.5
7	ss, muddy	<i>2.1</i>	<i>2.8</i>		<i>3.0</i>				2.8				3.4
11	ss, muddy	<i>4.4</i>	<i>2.9</i>		<i>3.1</i>				2.9				3.9
2	ss, silty	<i>2.0</i>	<i>3.3</i>		<i>3.5</i>				3.3				3.8
6	ss, silty	<i>2.5</i>	<i>2.8</i>		<i>3.0</i>				2.8				3.4
24	ss, silty	<i>4.8</i>	<i>3.8</i>		<i>3.9</i>				3.7				5.1
39	ss, silty	<u><i>10.0</i></u>	<i>2.7</i>		<i>2.5</i>				2.8		2.6		4.1
35	ss, silty (patchy)	<u><i>10.0</i></u>	<i>1.9</i>		<i>1.9</i>				2.1		2.1		3.1
30	ss/si	1.0	3.2	3.9	3.5	3.2	3.7	3.3	3.1	2.7	3.4	3.8	3.7
28	si	1.7		2.4	2.5	2.3	2.5	2.6		2.5	2.7	2.5	2.7
37	si to ms	<u><i>1.0</i></u>		2.6	3.2		2.6	3.0				2.6	3.4
29	si, muddy	1.3		2.6	2.5	2.1	2.2	2.4		2.5	2.6	2.2	2.7
31	si, muddy	1.3	2.2	2.3	2.4	2.3	2.6	2.7	2.4	2.4	2.6	2.6	2.6
1	si, muddy (joints)	<i>0.9</i>	<i>3.9</i>		<i>4.0</i>				3.8				4.2
40	si, sandy	<u><i>10.0</i></u>	<i>2.4</i>		<i>2.6</i>				2.5		2.6		4.3
32	si/ss (joints)	1.7	2.2	2.2	2.5	2.4	2.4	2.6	2.5	2.3	2.6	2.5	2.7

Sample orientation: “cm” measurement on the core mantle, “cb/ct” measurement on core top or bottom surface, “f” measurement along the core axis on a plane surface (flat). Italics mark values of *f*, which were calculated from cm. Porosity measurements: italics—Pudlo et al. (2012); underlined—estimates; all other—determined with water (Archimedes principle)

Table 4 Rock thermal properties derived for the different stratigraphic units (based on literature data (see text) and new measurements (Table 3) as well as well-log analogue analysis for boreholes with high-resolution temperature measurements)

	Quaternary				Tertiary			
	TC _B	TC _M	Hc	Por.	TC _B	TC _M	Hc	Por.
Sand	2.4	5.0	2.2	35	2.4	4.6	2.5	32
Silt	2.3	4.0	2.1	29	2.3	4.0	2.1	29
Clay	1.4	1.9	1.9	25	1.9	2.4	2.4	17
Marl/Till	2.1	3.1	2.0	24				
Coal	0.7	0.7	3.0	30				

	Cretaceous				Jurassic (Liassic)				Triassic (Exter & Arnstadt)				Triassic (Grabfeld & Erfurt)			
	TC _B	TC _M	Hc	Por.	TC _B	TC _M	Hc	Por.	TC _B	TC _M	Hc	Por.	TC _B	TC _M	Hc	Por.
Sandstone	3.4	5.6	2.0	23	3.4	5.6	2.0	23	2.4	3.4	2.1	22	2.4	3.0	2.3	13
Siltstone	2.5	3.2	2.4	15	2.5	3.2	2.4	15	2.5	3.2	2.4	15	2.5	2.9	2.5	10
Mudstone	2.2	3.2	2.2	23	2.5	3.5	2.4	19	2.5	3.5	2.4	19	1.7	1.9	2.3	9
Marlstone	2.1	2.4	2.3	10	2.1	2.4	2.3	10	1.9	2.2	2.3	10	2.1	2.3	2.4	6
Limestone	2.5	2.9	2.3	10												

	Triassic (Muschelkalk)				Triassic (U. Buntsandstein)				Triassic (M. & L. Bunt.)				Permian (Zechstein)			
	TC _B	TC _M	Hc	Por.	TC _B	TC _M	Hc	Por.	TC _B	TC _M	Hc	Por.	TC _B	TC _M	Hc	Por.
Sandstone					2.1	2.4	2.4	9	2.1	2.4	2.4	9				
Siltstone					1.8	2.0	2.6	8	1.8	2.0	2.6	8				
Mudstone	1.7	1.9	2.3	4	1.7	1.9	2.3	9	1.7	1.8	2.3	3	1.9	2.0	2.2	3
Marlstone	2.0	2.1	2.3	4	2.1	2.3	2.4	7								
Limestone	2.1	2.2	2.3	4									2.1	2.2	2.3	4
Anhydrite	3.2	3.3	2.7	2	3.2	3.3	2.7	2					3.2	3.3	2.7	2
Rock salt	5.0	5.0	1.8		5.0	5.0	1.8						5.4	5.4	1.8	

	Permian (sed. Rotliegend)				Permocarboniferous volcanic rocks			
	TC _B	TC _M	Hc	Por.	TC _B	TC _M	Hc	Por.
Sandstone	4.2	4.7	2.3	9				
Siltstone	2.6	2.8	2.1	2				
Mudstone	2.2	2.3	2.0	2				
Andesite					2.3	2.3	2.8	1
Rhyolite					2.9	3.0	2.5	1
Basalt					2.2	2.2	2.8	1

With TC_{B} bulk thermal conductivity ($W m^{-1} K^{-1}$), TC_{M} matrix thermal conductivity ($W m^{-1} K^{-1}$), Hc thermal capacity ($MJ m^{-3} K^{-1}$), $Por.$ porosity in per cent

matrix TC can be attributed to the respective mineral composition. Whereas the Cretaceous, Jurassic and Permian sandstones often show high quartz content, sandstone units of the Triassic contain large portions of feldspars and clay minerals of much lower TC than quartz. The matrix TC and bulk TC values for siltstones and mudstones show in general a similar trend but with less variability. Values of matrix TC and bulk TC are in the range of 1.8–3.5 and 1.7–2.6 $W m^{-1} K^{-1}$, respectively. Marlstones and limestones show,

due to their more homogeneous composition and porosity, the lowest variability in TC. The mean values of matrix TC and bulk TC of marlstones and limestones are 2.1 ± 0.2 and $2.4 \pm 0.3 W m^{-1} K^{-1}$, respectively.

The TD measurements performed on the Altmark samples were mainly conducted on mudstone and siltstone samples. Values of matrix heat capacity are in the order of $1.8 \pm 0.3 MJ m^{-3} K^{-1}$ and resemble values from literature (Table 4).

Table 5 Thermal units and assigned thermal properties

Unit	Main lithology	Matrix thermal conductivity ($\text{W m}^{-1} \text{K}^{-1}$)	Thermal capacity ($\text{MJ m}^{-3} \text{K}^{-1}$)	Heat production rate ($\mu\text{W m}^{-3}$)	Unit porosity (%)
1	Sand, silt, coal (lignite)	3.9	2.16	1.0	31.1
2	Clay, silt, sand	2.7	2.36	1.3	19.4
3	Silt, clay, sand	3.6	2.26	1.3	25.5
4	Marlstone, limestone, mudstone	2.6	2.29	1.0	11.0
5	Mudstone, sandstone, siltstone	4.1	2.25	1.5	18.9
6	Mudstone, siltstone, marlstone, sandstone	3.1	2.30	1.6	16.7
7	Mudstone, siltstone, marlstone	2.3	2.35	1.6	8.9
8	Limestone, marlstone, salt	2.4	2.25	1.0	3.6
9	Salt, mudstone, marlstone, anhydrite	3.2	2.19	1.8	4.7
10	Mudstone, siltstone, sandstone	1.9	2.39	1.8	5.0
11	Salt, anhydrite, mudstone	4.9	1.94	0.4	0.4
12	Sandstone, siltstone, mudstone	3.6	2.18	1.6	5.2
13	Ryholite, andesite	2.8	2.60	2.9	1.0
14	Greywacke, schist, limestone	3.1	2.30	2.8	1.0

Table 6 Layers of the 3-D thermal model

Layers	Thickness (m)	Depth range (m)
1–6	50	0–300
7–36	100	300–3,300
37–46	150	3,300–4,800
47	200	4,800–5,000
48–57	500	5,000–10,000

Subsurface temperature

The geological structure reflected in gentle anticlines and synclines and associated thickness changes of the geological units have a remarkable influence on the subsurface temperature distribution (Fig. 5). The isotherms in the W–E transect across the northern flank the Groß Gischau salt pillow (Fig. 5b) demonstrate the dependency of temperature and geological structure outside of thick salt accumulations (Fig. 5a). A gentle bending of isotherms above and below the moderately thick Zechstein salt is observed. The top salt has temperatures on the order of 90 °C being about 10 °C higher than temperatures at the eastern part of the section. At the base of the salt, temperature differences from west to east are subtle being on the order of 125 and 130 °C. More pronounced are the lateral temperature differences in the SE–NW transect (Fig. 5c), including the Apenburg and Lüge-Liesten salt diapirs. Here temperatures are significantly different above and within the salt dome, as well as beneath the salt compared to comparable depths in adjacent areas. Temperatures at the base of salt/top

Rotliegend reservoir range between 130 °C (in the west) and 150 °C (in the east). For most of the area outside the salt diapirs, temperatures at base of Mesozoic are on the order 100–110 °C.

Surface heat flow

Surface heat flow (q_s) resulting from the 3-D modelling shows consistent values of about 84–88 mW m^{-2} across the area (Fig. 6). At the S59 borehole location, the modelled q_s value is 90 mW m^{-2} . As expected from the rock thermal properties assigned to the model, the heat flow exceeds in areas, where large salt structures occur. For example, for the Lüge-Liesten diapir a, $q_s > 150 \text{ mW m}^{-2}$ may be expected for the top interval above the high heat-conducting salt. The areal extent of the high heat flow area is related to the salt dome thickness and diameter. For the salt diapirs, the disturbance of the heat flow is limited within an area of about 500 m around the outer rim of the salt dome. At the Apenburg salt structure, which is of a smaller size than the Lügen-Liesten diapir, q_s values are slightly lower and the areal extent of the q_s anomaly is less pronounced.

Discussion

The study aims at the quantification of subsurface temperatures for the larger Altensalzwedel area in dependence of the 3-D geological structure and heat diffusion through the sedimentary section. The temperature field and the q_s

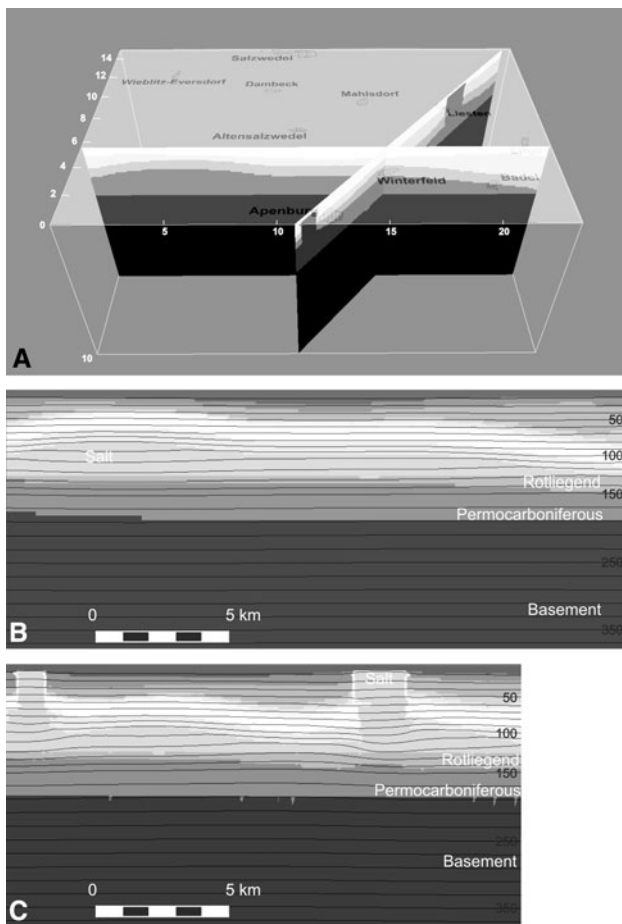
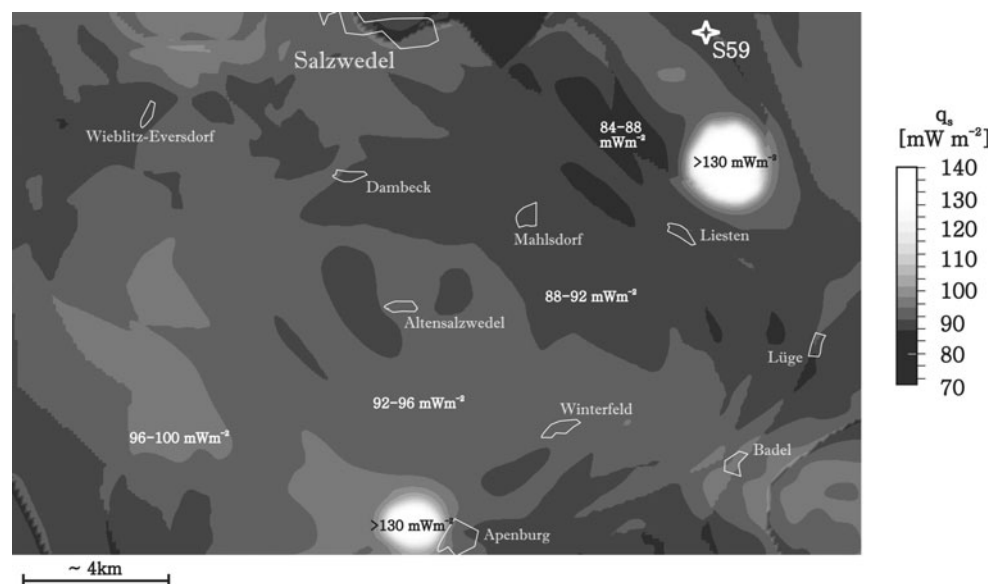


Fig. 5 Modelled temperature distribution along two sections of the 3-D model. **a** Location of the sections and simplified geological situation along the sections (*grey shaded*); **b** isotherms along the W–E transect, touching the salt pillow of Groß Gischau, geology is *grey-shaded*; **c** isotherms along the SW–NE transect across the salt diapirs at Apenburg and Lüge-Liesten, geology is *gray-shaded*

Fig. 6 Modelled surface heat flow (q_s in mW m^{-2}). Note the high values above salt structures



distribution resulting from the 3-D thermal model are affected by (1) the different rock thermal properties of the model domain, (2) the value selected as boundary heat flow at 10 km depth, and (3) the geological structure, especially the existence of salt accumulations of high thermal conductivity. For the latter, it is shown that thick Zechstein salt acts as a heat chimney, increasing the temperature in and above the salt and decreasing temperatures right below the salt structure. These observations are in line with earlier observations of local thermal anomalies around salt structures (e.g. Jensen 1990). In the NEGB, observations of this effect are documented by e.g. Hurtig and Rockel (1992) and Ondrak et al. (1998). Noack et al. (2010) and Magri et al. (2005) describe salt-dependent temperature and heat-flow anomalies at regional scale. Norden et al. (2008) quantified the extent of these salt-dependent thermal anomalies by 2-D and 3-D temperature models. In general, at a distance of <1 km from the outer rim of a salt dome, the disturbance of the temperature field is almost negligible. The results of this work were corroborated by Cacace et al. (2010) showing the zone of elevated q_s to be restricted to the immediate surroundings of the salt structure.

Whereas the structural setting and the sedimentary succession of the Altmark is well known and can explain local-scale thermal anomalies, the composition and the geological structure of the crust below 5 km are more speculative. However, changes in thickness and composition of crustal units may be responsible for large-scale variations of the thermal field and thus in q_s (e.g. Norden et al. 2008; Cacace et al. 2010). The modelled background q_s of $88\text{--}92 \text{ mW m}^{-2}$ of the larger Altensalzwedel area (Fig. 6, considered as crustal heat flow unaffected by heat

refraction at salt structures) is at the upper end of range previously reported for the NEGB ($68\text{--}91\text{ mW m}^{-2}$; mean value $77 \pm 3\text{ mW m}^{-2}$; Norden et al. 2008; Lotz 2004).

A better calibration of the thermal model would be possible with a larger amount of reliable temperature measurements. Unfortunately, the only continuous temperature log available as a model calibrator is the S59 log, Fig. 7. Also unfortunate is that no temperatures from drill-

stem tests were available for the study, which usually better approximate formation temperatures than BHTs. The corrected BHTs that we have used for the larger Altensalzwedel area (Lorenz 1971) are affected by a great uncertainty typical for this type of data. In the upper part of the section, BHTs are consistently lower than the temperatures of the S59 log. However, they approximate better with the modelled temperature at the respective borehole location

Fig. 7 Temperature logs of the S59 borehole and BHTs, measured (in *black*) versus modelled (in *red, dotted line*). The BHT data (Lorenz 1971) are from 7 boreholes west of the S59 borehole location (Fig. 3), covering an area of about 85 km^2 in the northern model domain; the lithology of the S59 borehole is indicated

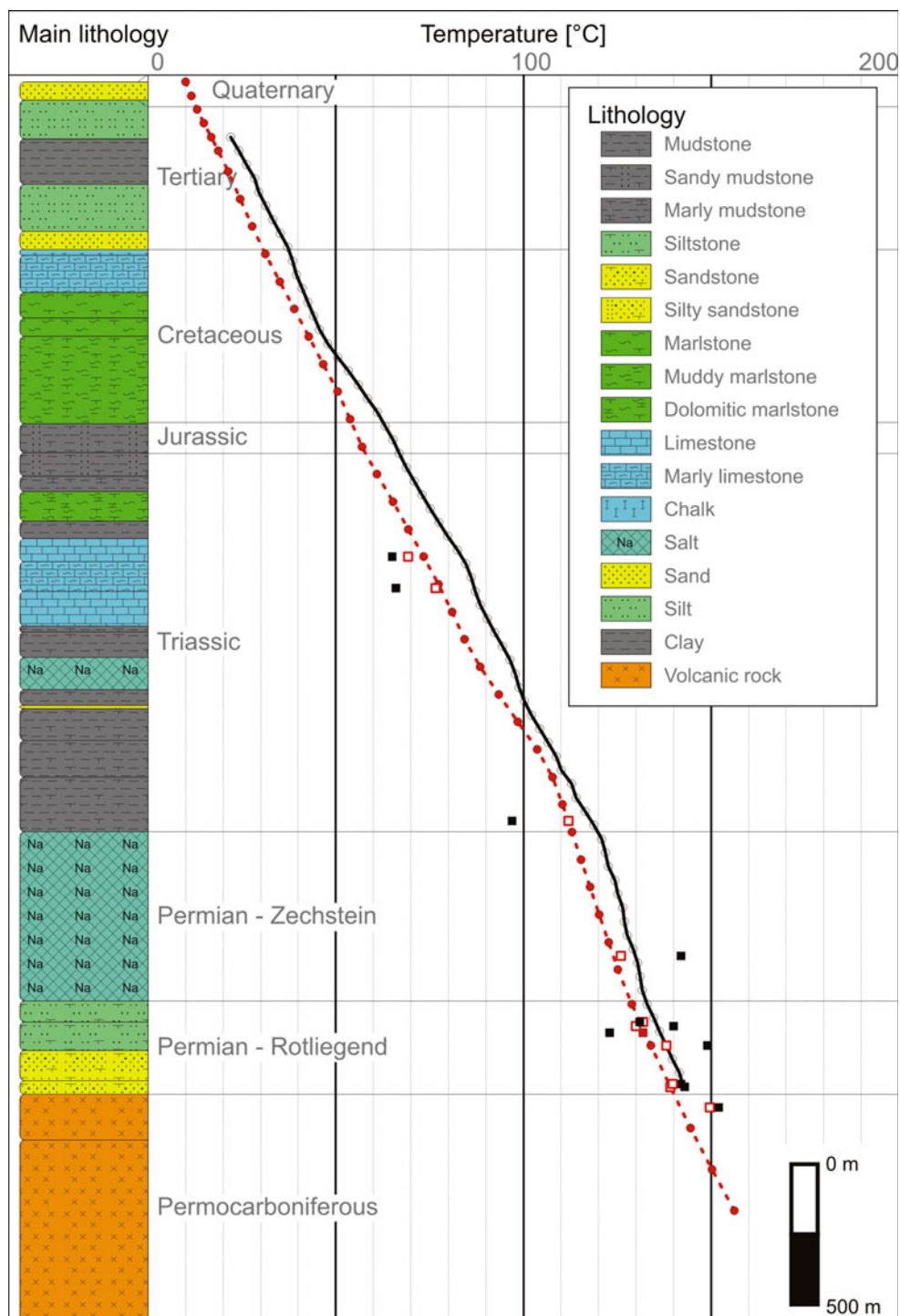


(Fig. 7). In the lower part of the section (>3,000 m), corrected BHTs are both higher and lower than the measured and the modelled temperature. Comparison of modelled and logged temperatures at the S59 site shows the modelled temperatures in general somewhat lower than the recorded values. The deviations are <10 °C.

There are two options for an improved fit of the model: (1) changing the boundary conditions as a regional factor or (2) changing the physical properties of the sedimentary section and/or of the basement, which could be a local factor. For the first case, higher temperatures (and q_s values) can be achieved by higher mantle heat-flow values resulting from a shallower lithosphere-asthenosphere boundary (e.g. the 1,300 °C isotherm) (Norden et al. 2008; Cacace et al. 2010). A further increase of boundary heat flow to values > 70 mW m⁻², however, is confronted with a resulting q_s value that would be higher than measured value.

In the second case, a higher heat-production rate for rhyolitic rocks or of the deeper basement rocks also would cause an increase of the heat flow. For example, Noack et al. (2012) show a thermal model assuming a 25-km-thick granitic upper crust with a mean heat production of 2.5 μW m⁻³ for the southern boundary of the State of Brandenburg, east of the Altmark (State of Sachsen-Anhalt) with typical lower crust practically absent. Such a 25-km-thick granitic unit would increase the basal heat flow at 10 km depth and the modelled temperatures of the

sediments but also the q_s . However, granite bodies of that thickness are unknown.

The most plausible way to fit the thermal model at the S59 location would be a modification of the TC data in the model, especially for the Mesozoic section between 600 and 2,700 m. However, the assignment of representative rock (or formation) thermal properties is the most difficult part in regional (or basin) geothermal modelling. In addition, care has to be taken on incorporating bulk rock values or matrix values into a numerical simulation, and if and how corrections to the calculated in situ temperature and pressure conditions are applied. The TC values used in Table 6 are related to matrix rock properties under ambient conditions. Mean bulk TC for different units take the unit porosity and the fluid content into account. In order to compare the assigned properties with data from Fuchs and Förster (2010) and data used by Bayer et al. (1997) and Noack et al. (2012), mean bulk thermal conductivities needs to be calculated. They range from 1.8 W m⁻¹ K⁻¹ for the muddy Lower and Middle Buntsandstein to 4.9 W m⁻¹ K⁻¹ for the Zechstein evaporites (Table 7). In general, the here used values are higher than those given by Bayer et al. (1997), especially for the Cenozoic, the Jurassic, and the Permian units. As Bayer et al. (1997) and Noack et al. (2012) do not apply corrections to in situ conditions, they do not distinguish between effective and ambient thermal conductivity values. Such an approach is justified as long as the increase of TC due to the increase of

Table 7 Comparison of applied formation thermal conductivities (TC), calculated for bulk TC (Bulk TC): (a) this study, (b) this study, temperature-corrected TC-values according to the formula of Zoth and Haenel (1988); (c) values from Bayer et al. (1997); (d) values

after Fuchs and Förster (2010), mean values in brackets, the asterisk denotes that Bulk TC values are available for parts of the Middle Buntsandstein, only; (e) values after Noack et al. (2012), model 3

Unit	Corresponding stratigraphy	Main lithology	Bulk TC (W m ⁻¹ K ⁻¹)				
			(a)	(b)	(c)	(d)	(e)
1	Quaternary to Tertiary (Chattian)	Sand, silt, coal (lignite)	2.1	2.1	1.5	n.a.	1.8
2	Tertiary (Rupelian)	Clay, silt, sand	2.0	2.0	1.5	n.a.	1.8
3	Tertiary (Eocene to Paleocene)	Silt, clay, sand	2.3	2.3	1.5	n.a.	1.8
4	Cretaceous	Marlstone, limestone, mudstone	2.2	2.1	1.9/2.0	2.6–3.0 (2.8)	3.04/2.71
5	Jurassic (Lias)	Mudstone, sandstone, siltstone	2.9	2.8	2.0	1.5–2.9 (2.3)	2.71
6	Keuper (Arnstadt & Exter Fm.)	Mudstone, siltstone, marlstone, sandstone	2.4	2.2	2.3	2.2–2.9 (2.5)	2.35
7	Keuper (Grabfeld & Erfurt Fm.)	Mudstone, siltstone, marlstone	2.1	1.8	2.3	1.9–2.0 (2.0)	2.35
8	Muschelkalk	Limestone, marlstone, salt	2.3	2.0	1.9	1.8–2.1 (2.0)	2.3
9	Upper Buntsandstein	Salt, mudstone, marlstone, anhydrite	3.0	2.7	2.0	1.8–2.2 (2.0)	2.58
10	Lower and Middle Buntsandstein	Mudstone, siltstone, sandstone	1.8	1.4	2.0	2.4–3.1 (2.8)*	2.58
11	Zechstein	Salt, anhydrite, mudstone	4.9	4.5	3.5	n.a.	4.5
12	Rotliegend	Sandstone, siltstone, mudstone	3.3	3.0	1.8–2.4	n.a.	3.3
13	Permian	Rhyolite, andesite	2.8	2.2	2.5	n.a.	2.5
14	Proterozoic to Westfalian (pre-Stefanian)	Greywacke, schist, limestone	3.1	2.2–2.5	2.0–3.0	n.a.	2.65–3.1

pressure versus depth is balanced off by the decrease of TC due to the increase of temperature versus depth. If, however, one effect is more pronounced, then this approach will fail in the prediction of temperatures. As it is stated by Kukkonen et al. (1999), the pressure effect is always minor (only about 10 % increase in TC takes place from surface to 35 km depth) in comparison to the temperature dependence of TC. Taking this observation into account, we corrected TC only for temperature using the formula implemented in the SHEMAT code (Table 7, column b). The formula is based on the relationship by Zoth and Haenel (1988) and is not calibrated to salt rocks. Therefore, the TC value for the Zechstein salt is most likely undercorrected in our modelling. By comparing these values with the values used by Bayer et al. (1997) and others, the differences of the respective in situ formation TC values decrease (Table 7).

Norden and Förster (2006) emphasise the dependence of formation TC on facies changes in a sedimentary basin. One should be aware of that the in situ TC values given by Fuchs and Förster (2010) (Table 7) are calculated from one specific borehole site. The values are both, higher and lower than the values used in this study. As the borehole used by Fuchs and Förster (2010) is located near Stralsund, about 200 km away from the study area, the differences in TC could reflect a different facies and mineralogy in the formations. The values used by Noack et al. (2012) in their model 3 were higher for the Cretaceous and for the Middle and Upper Triassic, and the Pre-Zechstein units (Table 7). Due to the high TC values used in that model, the temperatures calculated were lower than the measured temperatures and lower than a model using the lower TC values according to Bayer et al. (1997).

Given the immature state of knowledge on in situ formation and lithotype TC for the sediments in the NEGB and the uncertainties in crustal parameters we decided against a further calibration approach for the steady-state thermal model presented in this study. In addition, the calibration would be limited to only on one single continuous temperature log. It cannot be excluded that the S59 temperature log was measured under thermal borehole conditions not fully recovered from the temperature perturbations due to drilling and drill-mud and fluid circulation. This is indicated by temperatures >10 °C (the ambient ground temperature) near the surface.

Conclusions

The paper presents a quantification of the thermal field conditions to characterise in more detail the temperature to a depth of 10 km. The approach is novel as it concludes for the first time a comprehensive model of local geology,

including lithology, and a comprehensive data set of measured thermal rock properties. Even if the thermal model is regarded as a reconnaissance model, exhibiting some uncertainty pertaining to absolute temperatures, it forms a good basis on which local temperature prognoses can be made, for example, for predictions of the temperature path of planned boreholes and for the design of CO₂ injection regimes both of which are important engineering aspects.

With regard to geothermal utilizations, temperatures of about 140 °C in the Rotliegend reservoir at depths of about 3,500 m would be suitable for the production of electricity if appropriate fluid-flow rates could be achieved. Also shallower reservoirs may be considered for geothermal use as shown for other parts of the NEGB (Feldrappe et al. 2008; Wolfgramm et al. 2008). For example, the mapped temperatures at the base of the Mesozoic (at depths of $<2,000$ m) of about 100 °C may be of special interest if district heating is the focus.

In addition, the study highlights the importance of a proper in situ thermal rock property characterisation. Corrections of TC for in situ temperature and pressure need to be investigated further and integrated in geothermal studies.

Acknowledgments This study is part of the joint research project CLEAN, sponsored by the German Federal Ministry of Education and Research (BMBF) within the framework of the geoscientific research and development programme “GEOTECHNOLOGIEN”. This work is publication no. GEOTECH-1952. The authors would like to thank all partners of the CLEAN project for fruitful discussions. The manuscript benefitted from valuable comments of the editorial board and one anonymous reviewer.

References

- Bachmann GH, Ehling B-C, Eichner R, Schwab M (2008) Geologie von Sachsen-Anhalt. Schweizerbart, Stuttgart
- Balling N, Kristiansen JI, Breiner N, Poulsen KD, Rasmussen R, Saxov S (1981) Geothermal measurements and subsurface temperature modelling in Denmark. Techn Ber Geoskrifter No. 16: Dep of Geol Aarhus Univ, ISSN: 0105-824X
- Bayer U, Scheck M, Koehler M (1997) Modeling of the 3D thermal field in the Northeast German Basin. Geol Rundsch 86(2): 241–251
- Benek R, Kramer W, McCann T, Scheck M, Negendank J, Korich D, Huebscher H-D, Bayer U (1996) Permo-carboniferous magmatism of the Northeast German Basin. Tectonophysics 266: 379–404
- Benox D, Ludwig AO, Schulze W, Schwab G, Hartmann H, Knebel G, Januszewski I (1997) Struktur und Entwicklung mesozoischer Störungszonen in der Südwest-Altmark. Hallesches Jahrb Geowiss B19:83–114
- Cacace M, Kaiser BO, Lewerenz B, Scheck-Wenderoth M (2010) Geothermal energy in sedimentary basins: What we can learn from regional numerical models. Chem der Erde 70(S3):33–46
- Čermák V, Huckenholz H-G, Rybach L, Schmid R, Schopper JR, Schuch M, Stöffler D, Wohlenber J (1982) Physical properties of

- rocks. In: Augenheister G (ed) Landolt-Börnstein, vol 1a. Springer, Berlin
- Clauser C (2003) Numerical simulation of reactive flow in hot aquifers—Shemat and Processing Shemat. Springer, Berlin
- Deming D (1989) Application of bottom-hole temperature corrections in geothermal studies. *Geophysics* 18:775–786
- DSK (2002) German Stratigraphic Commission (ed) Stratigraphic Table of Germany 2002, Potsdam. ISBN:3-00-010197-7
- Effenberger H (2000) Dampferzeugung. Springer, Berlin
- El-Sharkawy AA, Rashed JH, Zaghloul MS, Ghoniem MH (1984) Study of thermal properties of polycrystalline KCl, KBr and HI in the temperature range 300 to 600 K. *Phys Stat Sol a* 85:429–434
- Feldrappe H, Obst K, Wolfgramm M (2008) Die mesozoischen Sandsteinaquifere des Norddeutschen Beckens und ihr Potential für die geothermische Nutzung. *Z Geol Wiss* 36(4–5):199–222
- Förster A (2001) Analysis of temperature data in the Northeast German Basin: continuous logs versus bottom-hole temperatures. *Petroleum Geosci* 7:241–254
- Fuchs S, Förster A (2010) Rock thermal conductivity of Mesozoic geothermal aquifers in the Northeast German Basin. *Chem der Erde* 70(S3):13–22
- Hamdan IN, Clarke BG (2010) Determination of thermal conductivity of coarse and fine sand soils. In: Proc World Geotherm Congr, vol 7, Bali, Indonesia, 25–29 April 2010
- Haszeldine RS (2009) Carbon capture and storage: how green can black be? *Science* 325:1647–1652. doi:10.1126/science.1172246
- Hjuler ML, Fabricius IL (2009) Engineering properties of chalk related to diagenetic variations of Upper Cretaceous onshore and offshore chalk in the North Sea area. *J Petroleum Sci Eng* 68:151–170
- Höiting B (1996) Hydrogeologie. Enke, Stuttgart
- Hurtig E, Rockel W (1992) Federal Republic of Germany Eastern Federal States. In: Hurtig E, Čermák V, Haanel R, Zui V (eds) Geothermal atlas of Europe. Hermann Haack Verlagsgesellschaft mbH, Gotha, pp 38–40
- Jensen P (1990) Analysis of the temperature field around salt diapirs. *Geothermics* 19(3):273–283
- Jessop A (1990) Comparison of industrial and high-resolution thermal data in sedimentary basin. *Pure Appl Geophys* 133:251–267
- Kühn M, Bartels J, Iffland J (2002) Predicting reservoir property trends under heat exploitation: interaction between flow, heat transfer, transport, and chemical reactions in a deep aquifer at Stralsund, Germany. *Geothermics* 31:725–749
- Kühn M, Förster A, Großmann J, Meyer R, Reinicke K, Schäfer D, Wendel H (2011) CLEAN: preparing for a CO₂-based enhanced gas recovery in a depleted gas field in Germany. *Energy Procedia* 4:5520–5526. doi:10.1016/j.egypro.2011.02.538
- Kühn M, Tesmer M, Pilz P, Meyer R, Reinicke K, Förster A, Kolditz O, Schäfers D, CLEAN Partners (2012) CLEAN: CO₂ Large-Scale Enhanced Gas Recovery in the Altmark Natural Gas Field (Germany): Project overview. *Environ Earth Sci*. doi:10.1007/s12665-012-1714-z
- Kukkonen I, Jokinen J, Seipold U (1999) Temperature and pressure dependencies of thermal transport properties of rocks: implications for uncertainties in thermal lithosphere models and new laboratory measurements of high-grade rocks in the Central Fennoscandian Shield. *Surv Geophys* 20:33–59
- LAGB (2011) Tektonische Übersichtskarte C3130 Salzwedel. Landesamt für Geologie und Bergwesen Sachsen-Anhalt (Geo Surv of Saxony-Anhalt). <http://webs.idu.de/lagb/lagb-default.asp?thm=tek400&tk=C3130>. Accessed 10 Nov 2011
- LBEG (2010) Erdöl und Erdgas in der Bundesrepublik Deutschland 2009. Landesamt für Bergbau, Energie und Geologie Niedersachsen (Geo Surv of Lower Saxony), Hannover
- Lorenz J (1971) Beitrag zum Zusammenhang von Geothermie, Geochemie und Hydrodynamik im Rotliegenden des Gebietes Salzwedel-Marnitz sowie NE-Mecklenburgs. Bergakademie Freiberg (unpublished report)
- Lotz B (2004) Neubewertung des rezenten Wärmestroms im Nordostdeutschen Becken. Sci Tech Rep, GeoForschungsZentrum Potsdam, STR Rep 04/04: ISSN: 1610-0956
- Magri F, Bayer U, Jahnke C, Clausnitzer V, Diersch H, Fuhrman J, Moeller P, Pekdeger A, Tesmer M, Voigt H (2005) Fluid-dynamics driving saline water in the North East German Basin. *Int J Earth Sci* 94(5):1056–1069
- Mottaghy D, Pechinig R (2009) Numerische 3-D Modelle zur Temperaturvorhersage und Reservoirsimulation. *BBR Fachmagazin für Brunnen- und Leitungsbau* 10:44–51
- Müller EP (1994) Development of oil and gas exploration in the eastern part of Germany. In: Popescu BM (ed) Hydrocarbons of Eastern Central Europe. Springer, Heidelberg, pp 119–146
- Noack V, Cherubini Y, Scheck-Wenderoth M, Lewerenz B, Höding T, Simon A, Moeck I (2010) Assessment of the present-day thermal field (NE German Basin)—inferences from 3D modeling. *Chem der Erde* 70:47–62
- Noack V, Scheck-Wenderoth M, Cacace M (2012) Sensitivity of 3D thermal models to the choice of boundary conditions and thermal properties: a case study for the area of Brandenburg (NE German Basin). *Environ Earth Sci*. doi:10.1007/s12665-012-1614-2
- Norden B, Förster A (2006) Thermal conductivity and radiogenic heat production of sedimentary and magmatic rocks in the Northeast German Basin. *AAPG Bull* 90(6):939–962
- Norden B, Förster A, Balling N (2008) Heat flow and lithospheric thermal regime in the Northeast German Basin. *Tectonophysics* 460:215–229
- Ondrak R, Wenderoth F, Scheck M, Bayer U (1998) Integrated geothermal modeling on different scales in the Northeast German basin. *Geol Rundsch* 87:32–42
- Otto R (2010) Bestimmung von Wärmeleitfähigkeiten. Abstract, 70. Jahrestagung der Dtsch Geophysikalischen Ges March 2010, Bochum
- Pechinig R, Arnold J, Jorand R, Koch A, Clauser C (2009) Ergebnisse einer integrierten Analyse von Labor- und Bohrlochmessdaten an Lockersedimenten der Niederrheinischen Bucht und Festgesteinen des Rheinischen Schiefergebirges. In: Proceedings 5th NRW-Geothermiekonf Bochum November 2009
- Popov YA, Pribnow DFC, Sass JH, Williams CF, Burkhardt H (1999) Characterization of rock thermal conductivity by high resolution optical scanning. *Geothermics* 28:253–276
- Pudlo D, Reitenbach V, Albrecht D, Ganzer L, Gernert U, Wienand J, Kohlhepp B, Gaupp R (2012) The impact of diagenetic fluid-rock reactions on Rotliegend sandstone composition and petrophysical properties (Altmark area, central Germany). *Environ Earth Sci*. doi:10.1007/s12665-012-1723-y
- Radzinski KH (1996) Erdgeschichtlicher Rückblick, Sachsen-Anhalt. In: Das Geologische Landesamt—Tätigkeitsbericht 1993 bis 1995, Geo Surv Halle, pp 11–18
- Rückheim J, Voigtländer G, Stein-Khokhlov M (2005) The technical and economic challenge of “mature gas fields”: the giant Altmark Field, a German example. *SPE 94406, SPE/EAGE annual conference Madrid*, pp 659–662
- Scheibe R, Seidel K, Vormbaum M, Hoffmann N (2005) Magnetic and gravity modelling of the crystalline basement in the North German Basin. *Z dt Ges Geowiss* 156:291–298
- Schön J (1996) Physical properties of rocks: fundamentals and principles of petrophysics. In: Helbig K, Teitel S (eds) *Handb Geophy Explor*, Sect. 1, 18
- Speece M, Bowen T, Folcik J, Polack H (1985) Analysis of temperatures in sedimentary basins: the Michigan Basin. *Geophysics* 50:1318–1334
- Stottmeister L, von Pöbloski B (1999) Die geologische Entwicklung der Altmark—eine Übersicht. *Mitt Geol Sachsen-Anhalt* 5:45–72

- Stottmeister L, von Poblozki B, Reichenbach W (2008) Altmark-Fläming-Scholle. In: Bachmann GH, Ehling B-C, Eichner R, Schwab M (eds) *Geologie von Sachsen-Anhalt*. Schweizerbart, Stuttgart, pp 348–369
- Trusheim F (1957) Über Halokinese und ihre Bedeutung für die strukturelle Entwicklung Norddeutschlands. *Z Dtsch Geol Ges* 109:111–151
- TU München (ed) (2010) Bavarian online material information system. <http://www.werkstoffe.de>. Accessed 15 Nov 2010
- UEIS (2010) Berlin Digital Environmental Atlas. Urban and environmental information system (UEIS). Department for Urban Development, Berlin. http://www.stadtentwicklung.berlin.de/umwelt/umweltatlas/edua_index.shtml. Accessed 16 Nov 2010
- VDI (2000) VDI 4640—thermal use of the underground, Part 1 & 2. VDI Man Energy Techn, Düsseldorf
- Vedova BD, Vecellio C, Bellani S, Tinivella U (2008) Thermal modelling of the Larderello geothermal field (Tuscany, Italy). *Int J Earth Sci (Geol Rundsch)* 97:317–332. doi:10.1007/s00531-007-0249-0
- Wolfgramm M, Rauppach K, Seibt P (2008) Reservoir-geological characterization of Mesozoic sandstones in the North German Basin by petrophysical and petrographical data. *Z Geol Wiss* 36(4–5):249–265
- Ziegler PA (1990) *Geological atlas of Western and Central Europe*. Shell Internationale Petroleum Maatschappij B.V., New York, pp 1–239
- Zoth G, Haenel R (1988) Thermal conductivity. In: Haenel R, Rybach L, Stegena L (eds) *Handbook of terrestrial heat-flow density determination*. Kluwer Academic Publishers, Norwell, pp 449–453